Frontiers of Information Technology & Electronic Engineering
www.jzus.zju.edu.cn engineering.cae.cn www.springerlink.com
ISSN 2095-9184 (print); ISSN 2095-9230 (online)
E-mail: jzus@zju.edu.cn

Near-field secure wireless communication with delay alignment modulation*

Haiquan LU[1,2], Yong ZENG‡[1,2]

[1]*National Mobile Communications Research Laboratory, Frontiers Science Center for Mobile Information Communication and Security, Southeast University, Nanjing 210096, China*

[2]*Purple Mountain Laboratories, Nanjing 211111, China*

E-mail: haiquanlu@seu.edu.cn; yong_zeng@seu.edu.cn

Received Apr. 10, 2024; Revision accepted Aug. 8, 2024; Crosschecked Sept. 29, 2024; Published online Dec. 7, 2024

Abstract: Delay alignment modulation (DAM) is recently proposed as an effective technique to address the inter-symbol interference (ISI) issue, which circumvents the conventional channel equalization and multi-carrier transmission. Moreover, wireless communications are vulnerable to malicious eavesdropping and attacks due to their inherent open and broadcast nature. In particular, DAM not only eliminates the ISI at the desired receiver but may also introduce ISI to other locations, and thus is quite promising for secure communications. This paper considers the near-field secure wireless communication with DAM. To gain useful insights, it is first shown that when the antenna number of Alice is much larger than the number of multipaths for Bob and Eve, the delay compensation and low-complexity path-based maximal-ratio transmission (MRT) beamforming achieve a communication free of ISI and information leakage, owing to the asymptotically orthogonal property brought by the near-field nonuniform spherical wave (NUSW). The secrecy rate performance of path-based zero-forcing (ZF) beamforming toward ISI-free communication is then evaluated. Furthermore, the path-based optimized DAM beamforming scheme is proposed to maximize the secrecy rate, by considering the general case in the presence of some tolerable ISI. As a comparison, the benchmarking scheme of the artificial noise (AN) based orthogonal frequency-division multiplexing (OFDM) is considered. Simulation results show that DAM achieves a higher secrecy rate and lower peak-to-average-power ratio (PAPR) than the AN-based OFDM.

Key words: Near-field; Nonuniform spherical wave; Delay alignment modulation (DAM); Inter-symbol interference (ISI) free communication; Physical layer security; Secrecy rate

https://doi.org/10.1631/FITEE.2400271 **CLC number:** TN929.5

1 Introduction

By taking advantage of the super-spatial resolution of the extremely large-scale array (XL-array) (Lu et al., 2024b) and the multipath sparsity of millimeter wave (mmWave) and terahertz (THz) channels, delay alignment modulation (DAM) emerges as an effective inter-symbol interference (ISI) mitigation technique via spatial-delay processing (Lu and Zeng, 2022b). The essential idea of DAM lies in "path delay compensation and path-based beamforming." More concretely, by deliberately introducing the delay matching with each individual channel path and combining with path-based beamforming, all multipath signal components arrive at the receiver in a simultaneous and constructive manner, instead of giving rise to the detrimental ISI. As a result, an ISI-free additive white Gaussian noise (AWGN) channel is obtained, which removes the need for the sophisticated channel

‡ Corresponding author

* Project supported by the Natural Science Foundation for Distinguished Young Scholars of Jiangsu Province, China (No. BK20240070), the National Natural Science Foundation of China (No. 62071114), and the Fundamental Research Funds for the Central Universities (No. 2242022k60004)

ORCID: Haiquan LU, https://orcid.org/0000-0002-3897-9950; Yong ZENG, https://orcid.org/0000-0002-3670-0434

equalization or multi-carrier transmissions, and thus, DAM is quite effective for broadband frequency-selective systems with large antenna arrays. Further, a DAM-based manipulable channel delay spread architecture was established (Lu and Zeng, 2023), thus enabling efficient single- or multi-carrier transmissions. Furthermore, for the more challenging doubly selective channel, DAM was extended to the delay-Doppler alignment modulation (DDAM) (Lu and Zeng, 2024), so as to achieve Doppler-ISI dual mitigation. In particular, the single-carrier DAM/DDAM notably saves the guard interval compared to orthogonal frequency-division multiplexing (OFDM), and thus a higher spectral efficiency is expected, yet with a lower peak-to-average-power ratio (PAPR). The recent research efforts on DAM include mainly channel estimation (Ding et al., 2024), multiuser communications (Wang XW et al., 2023), intelligent reflecting surface (IRS) aided communications (Lu et al., 2024a; Sun et al., 2024), hybrid beamforming implementation (Zhang JN and Zeng, 2024), and integrated sensing and communication (ISAC) (Hao et al., 2023; Xiao and Zeng, 2023; Wang ZL et al., 2024).

In addition to the ISI issue caused by the multipath propagation, the open and broadcast nature of wireless environment renders legitimate communications susceptible to malicious eavesdropping and attacks (Mukherjee et al., 2014; Zou et al., 2016; Liu Y et al., 2023). To safeguard wireless communication against security threats, one commonly used approach is to leverage the secret key based cryptographic techniques at the upper layers. Despite the effectiveness, the use of cryptographic techniques involves encryption and decryption procedures, which imposes a computation burden on devices and causes communication latency (Yang et al., 2015; Zou et al., 2016). As a complementary technique, physical layer security makes use of the randomness of wireless propagation channels to strengthen the resistance to eavesdropping, without resorting to cryptographic techniques (Dong L et al., 2010; Mukherjee et al., 2014), thus enabling a new paradigm for enhancing the security. The typical technologies of physical layer security consist of artificial noise (AN), security-oriented beamforming, cooperative relay (Dong L et al., 2010; Zou et al., 2016), directional modulation (Hong et al., 2011), and so on. Moreover, numerous efforts have been devoted to physical layer security in various application scenarios, such as massive multiple-input multiple-output (MIMO) communications (Zhu et al., 2014), unmanned aerial vehicle (UAV) aided communications (Zhang GC et al., 2019), IRS/reconfigurable intelligent surface (RIS) aided communications (Cui M et al., 2019; Zhou G et al., 2021; Liu YW et al., 2023; Illi et al., 2024), and near-field communications (Chen et al., 2024; Ferreira et al., 2024).

It is worth mentioning that existing AN-based physical layer security schemes increase the disparity between legitimate and eavesdropping links by sacrificing part of the power for transmitting the AN. On the other hand, DAM achieves ISI elimination at the desired receiver, while for other locations with different spatial signatures from the receiver, it inherently causes ISI. Such an ISI may play the same role as the AN to degrade the eavesdropping link without sacrificing the transmit power, rendering DAM quite promising for secure transmissions. Moreover, the deployment of XL-array for DAM enables a paradigm shift from far-field communications to near-field communications (Cui MY and Dai, 2022; Lu and Zeng, 2022a; Zhang HY et al., 2022), for which the more general nonuniform spherical wave (NUSW) based channel model should be considered (Lu et al., 2024b). Compared to the far-field uniform plane wave (UPW), the near-field NUSW achieves the evolution from beam-steering to beam-focusing (Zhang HY et al., 2022; Li et al., 2024; Lu et al., 2024b), which endows DAM a higher spatial resolution to distinguish the multipath signal components. Note that in addition to the conventional discrete antenna array, many works have concentrated on continuous-aperture holographic MIMO near-field communications (Wei et al., 2023; Gong et al., 2024), as well as on RIS-aided near-field communications (Cheng et al., 2024).

Motivated by the above observations, this paper studies the near-field secure multiple-input single-output (MISO) communication with DAM, by focusing on the conventional discrete antenna array. The main contributions of this paper are as follows:

First, for the asymptotic case, when the antenna number of Alice is much larger than the number of multipaths for Bob and Eve, it is shown that without relying on the channel state information (CSI) of Eve, DAM achieves an "ISI-free and information

leakage-free communication" with delay precompensation and low-complexity path-based maximal-ratio transmission (MRT) beamforming. Moreover, when the number of antennas for Alice is not smaller than the multipath number for Bob, an ISI-free communication can be obtained with path-based zero-forcing (ZF) beamforming, while introducing ISI to Eve simultaneously. The secrecy rate of path-based ZF beamforming is then evaluated.

Second, by tolerating some ISI, the path-based beamforming is optimized to maximize the secrecy rate, and the successive convex approximation (SCA) technique is used to efficiently solve the nonconvex problem. For comparison, the benchmarking scheme of the AN-based OFDM scheme is considered. Compared to AN-based OFDM, DAM secure communication not only avoids allocating the dedicated power to AN but also saves the guard interval. Simulation results verify the performance gain of DAM over AN-based OFDM in terms of secrecy rate and PAPR, as well as the importance of taking into account the NUSW-based model in near-field communications.

Notations: $(\cdot)^{\mathrm{T}}$ and $(\cdot)^{\mathrm{H}}$ denote the transpose and Hermitian transpose, respectively. The distribution of a circularly symmetric complex Gaussian random variable with zero mean and variance σ^2 is denoted by $\mathcal{CN}\left(0,\sigma^2\right)$. The symbol j denotes the imaginary unit of complex numbers, with $\mathrm{j}^2=-1$. The notation $\circledast$ represents the linear convolution. $\mathbb{E}\left[\cdot\right]$ represents the statistical expectation, and $\mathrm{Re}\left\{\cdot\right\}$ represents the real part of the complex number. $\mathcal{O}$ stands for the standard big-O notation.

2 System model

As shown in Fig. 1, we consider a near-field MISO communication system, where a transmitter (Alice) communicates with a single-antenna legitimate receiver (Bob) in the presence of a single-antenna eavesdropper (Eve). Alice is equipped with an XL uniform linear array (XL-ULA) with M ($M\gg 1$) isotropic antennas. Without loss of generality, XL-ULA is centered at the origin and placed along the y axis. The location of the m^{th} antenna is $\boldsymbol{w}_m=[0,\delta_m d]^{\mathrm{T}}$, where $\delta_m=(2m-M-1)/2$, $m=1,2,\cdots,M$, and d denotes the antenna spacing. Let L_{B} denote the number of temporal-resolvable multipaths between Alice and Bob, with each multipath

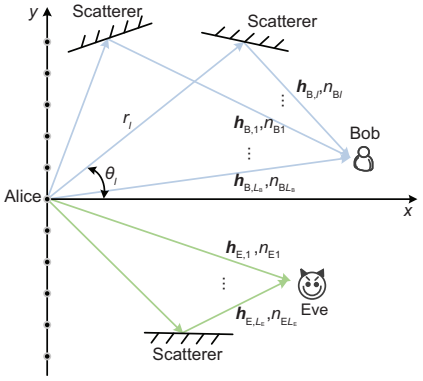

Fig. 1 A near-field secure communication system

corresponding to one scatterer. For the line-of-sight (LoS) path, the scatterer can be treated as Bob itself. The location of scatterer l is $\boldsymbol{q}_l=[r_l\cos\theta_l, r_l\sin\theta_l]^{\mathrm{T}}$, where $1\le l\le L_{\mathrm{B}}$, r_l denotes the distance between the center of the XL-ULA and the corresponding scatterer, and θ_l denotes the angle between the line segment connecting the array center and the scatterer relative to the x axis. Thus, the distance between the m^{th} antenna and the l^{th} scatterer is

$$r_{l,m}=\left\|\boldsymbol{w}_m-\boldsymbol{q}_l\right\|=\sqrt{r_l^2-2r_l\delta_m d\sin\theta_l+\delta_m^2 d^2}. \tag{1}$$

With the near-field NUSW model that accurately takes into account both the phase and the amplitude variations across array elements, the transmit array response vector of the multipath l between Alice and Bob is as follows (Lu and Zeng, 2022a; Lu et al., 2024b):

$$\begin{aligned}&\boldsymbol{a}_{\mathrm{B}}\left(r_l,\theta_l\right)\\&=\left[\frac{r_l}{r_{l,1}}\mathrm{e}^{-\mathrm{j}\frac{2\pi}{\lambda}\left(r_{l,1}-r_l\right)},\ \cdots,\ \frac{r_l}{r_{l,M}}\mathrm{e}^{-\mathrm{j}\frac{2\pi}{\lambda}\left(r_{l,M}-r_l\right)}\right]^{\mathrm{T}}.\end{aligned} \tag{2}$$

The spatially stationary channel vector of multipath l is $\boldsymbol{h}_{\mathrm{B},l}\in\mathbb{C}^{M\times 1}=\alpha_{\mathrm{B}l}\boldsymbol{a}_{\mathrm{B}}\left(r_l,\theta_l\right)$, with $\alpha_{\mathrm{B}l}$ denoting the complex-valued gain. Under the quasistatic block-fading model, the discrete-time equivalent of the channel impulse response (CIR) from Alice to Bob is

$$\boldsymbol{h}_{\mathrm{B}}\left[n\right]=\sum_{l=1}^{L_{\mathrm{B}}}\boldsymbol{h}_{\mathrm{B},l}\delta\left[n-n_{\mathrm{B}l}\right], \tag{3}$$

where $n_{\mathrm{B}l}$ denotes the discretized delay. Similarly, CIR of the eavesdropping channel from Alice to Eve is

$$\boldsymbol{h}_{\mathrm{E}}\left[n\right]=\sum_{l=1}^{L_{\mathrm{E}}}\boldsymbol{h}_{\mathrm{E},l}\delta\left[n-n_{\mathrm{E}l}\right], \tag{4}$$

where L_{E} denotes the number of temporal-resolvable multipaths between Alice and Eve, $\boldsymbol{h}_{\mathrm{E},l} \in \mathbb{C}^{M\times 1}$ denotes the channel vector of multipath l between Alice and Eve, and $n_{\mathrm{E}l}$ denotes the corresponding discretized delay. Let $n_{a,\max} \triangleq \max\limits_{1\le l\le L_a} n_{al}$ and $n_{a,\min} \triangleq \min\limits_{1\le l\le L_a} n_{al}$ denote the maximum and minimum delays, respectively, over L_a multipaths, with $a \in \{\mathrm{B},\mathrm{E}\}$. Note that for the more general time-variant frequency-selective channel, DAM can be extended to DDAM for achieving the Doppler-ISI dual mitigation (Lu and Zeng, 2024).

With DAM, the transmitted signal of Alice is (Lu and Zeng, 2022b)

$$\boldsymbol{x}[n] = \sum_{l=1}^{L_{\mathrm{B}}} \boldsymbol{f}_l s[n-\kappa_l], \tag{5}$$

where $\boldsymbol{f}_l \in \mathbb{C}^{M\times 1}$ denotes the path-based beamforming, and $\kappa_l \ge 0$ is the deliberately introduced delay for the symbol sequence, with $\kappa_l \ne \kappa_{l'}$, $\forall l \ne l'$. For the practical implementation of DAM, delay compensation by κ_l simply corresponds to the time shift of the sequence of $s[n]$, and path-based beamforming can be implemented similar to standard beamforming techniques. The transmit power of Eq. (5) is $\mathbb{E}[\|\boldsymbol{x}[n]\|^2] = \sum_{l=1}^{L_{\mathrm{B}}} \|\boldsymbol{f}_l\|^2 \le P$, where P represents the maximum power available at Alice. The received signal at Bob is

$$\begin{aligned} y_{\mathrm{B}}[n] =& \boldsymbol{h}_{\mathrm{B}}^{\mathrm{H}}[n] \circledast \boldsymbol{x}[n] + z_{\mathrm{B}}[n] \\ =& \sum_{l=1}^{L_{\mathrm{B}}} \boldsymbol{h}_{\mathrm{B},l}^{\mathrm{H}} \boldsymbol{f}_l s[n-\kappa_l-n_{\mathrm{B}l}] \\ &+ \sum_{l=1}^{L_{\mathrm{B}}} \sum_{l'=1,l'\ne l}^{L_{\mathrm{B}}} \boldsymbol{h}_{\mathrm{B},l}^{\mathrm{H}} \boldsymbol{f}_{l'} s[n-\kappa_{l'}-n_{\mathrm{B}l}] + z_{\mathrm{B}}[n], \end{aligned} \tag{6}$$

where $z_{\mathrm{B}}[n] \sim \mathcal{CN}(0,\sigma^2)$ is the AWGN. By letting $\kappa_l = n_{\mathrm{B},\max} - n_{\mathrm{B},l}$, $\forall l \in \{1,2,\ldots,L_{\mathrm{B}}\}$, we have

$$\begin{aligned} & y_{\mathrm{B}}[n] \\ =& \underbrace{\left(\sum_{l=1}^{L_{\mathrm{B}}} \boldsymbol{h}_{\mathrm{B},l}^{\mathrm{H}} \boldsymbol{f}_l\right) s[n-n_{\mathrm{B},\max}]}_{\text{desired signal}} \\ &+ \underbrace{\sum_{l=1}^{L_{\mathrm{B}}} \sum_{l'=1,l'\ne l}^{L_{\mathrm{B}}} \boldsymbol{h}_{\mathrm{B},l}^{\mathrm{H}} \boldsymbol{f}_{l'} s[n-n_{\mathrm{B},\max}+\Delta_{\mathrm{B}l',\mathrm{B}l}]}_{\text{ISI}} \\ &+ z_{\mathrm{B}}[n], \end{aligned} \tag{7}$$

where $\Delta_{\mathrm{B}l',\mathrm{B}l} \triangleq n_{\mathrm{B}l'} - n_{\mathrm{B}l}$ denotes the delay difference between path l' and path l for Bob. Moreover, the received signal at Eve is

$$\begin{aligned} y_{\mathrm{E}}[n] =& \boldsymbol{h}_{\mathrm{E}}^{\mathrm{H}}[n] \circledast \boldsymbol{x}[n] + z_{\mathrm{E}}[n] \\ =& \sum_{l=1}^{L_{\mathrm{E}}} \sum_{l'=1}^{L_{\mathrm{B}}} \boldsymbol{h}_{\mathrm{E},l}^{\mathrm{H}} \boldsymbol{f}_{l'} s[n-n_{\mathrm{B},\max}+\Delta_{\mathrm{B}l',\mathrm{E}l}] + z_{\mathrm{E}}[n], \end{aligned} \tag{8}$$

where $\Delta_{\mathrm{B}l',\mathrm{E}l} \triangleq n_{\mathrm{B}l'} - n_{\mathrm{E}l}$ denotes the delay difference between path l' of Bob and path l of Eve.

3 ISI-free DAM secure communication

In this section, we study the ISI-free DAM secure communication by designing the path-based beamforming. To gain useful insights, we first provide an asymptotic analysis by assuming that $M \gg L_{\mathrm{B}}$ and $M \gg L_{\mathrm{E}}$, which will become more feasible due to the developing trends of XL-array and mmWave/THz communications with multipath sparsity for the sixth-generation (6G) wireless network.

3.1 Near-field asymptotic analysis

Let $\rho_{l,l'} \triangleq \frac{\left|\boldsymbol{h}_l^{\mathrm{H}} \boldsymbol{h}_{l'}\right|^2}{\|\boldsymbol{h}_l\|^2 \|\boldsymbol{h}_{l'}\|^2}$ denote the absolute square of the normalized inner product between channel vectors $\boldsymbol{h}_l$ and $\boldsymbol{h}_{l'}$, where $\boldsymbol{h}_l$ can be $\boldsymbol{h}_{\mathrm{B},l}$ or $\boldsymbol{h}_{\mathrm{E},l}$. With the near-field NUSW model in Eq. (2), we have

$$\begin{aligned} \rho_{l,l'} &= \frac{\left|\boldsymbol{a}^{\mathrm{H}}(r_l,\theta_l)\,\boldsymbol{a}(r_{l'},\theta_{l'})\right|^2}{\|\boldsymbol{a}(r_l,\theta_l)\|^2 \|\boldsymbol{a}(r_{l'},\theta_{l'})\|^2} \\ &= \frac{\left|\sum\limits_{m=1}^{M} \frac{1}{r_{l,m} r_{l',m}} \mathrm{e}^{\mathrm{j}\frac{2\pi}{\lambda}\left(r_{l,m}-r_{l',m}\right)}\right|^2}{\left(\sum\limits_{m=1}^{M} \frac{1}{r_{l,m}^2}\right)\left(\sum\limits_{m=1}^{M} \frac{1}{r_{l',m}^2}\right)}. \end{aligned} \tag{9}$$

It is difficult to directly obtain the closed-form expression of Eq. (9), but its value can be obtained numerically. Fig. 2 shows the near-field NUSW-based value for $\rho_{1,2}$ versus the number of antenna elements M, with $(r_1,\theta_1) = (30\ \mathrm{m}, 0^\circ)$ and $(r_2,\theta_2) = (45\ \mathrm{m}, \theta_1+\Delta\theta)$. It is observed that $\rho_{1,2}$ exhibits a decreasing trend as M increases, even when the two channel vectors have a common signal direction, i.e., $\Delta\theta = 0^\circ$. This indicates that the near-field channel vectors tend to be asymptotically orthogonal when the antenna number is much larger than that of the multipaths. Such a result eases the requirement for

different channel vectors with distinct angles of departure (AoDs) in the far-field region (Lu and Zeng, 2023), due to the super-spatial resolution brought by XL-ULA.

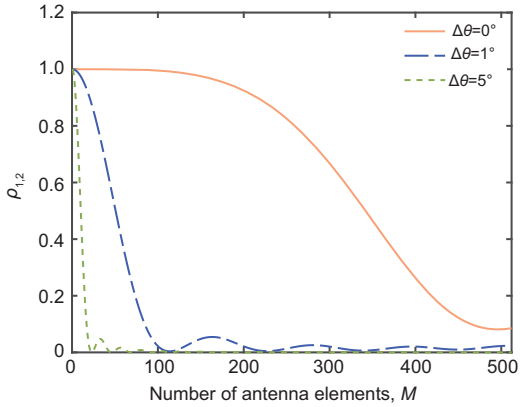

Fig. 2 Absolute square of the normalized inner product for two near-field channel vectors, where $(\boldsymbol{r}_1, \boldsymbol{\theta}_1) = (30\ \mathrm{m}, 0^\circ)$ and $(\boldsymbol{r}_2, \boldsymbol{\theta}_2) = (45\ \mathrm{m}, \boldsymbol{\theta}_1 + \boldsymbol{\Delta\theta})$

As a result, for the asymptotic case when $M \gg L_\mathrm{B}$ and $M \gg L_\mathrm{E}$, we have

$$\frac{\boldsymbol{h}_{\mathrm{B},l}^\mathrm{H}\boldsymbol{h}_{\mathrm{B},l'}}{\|\boldsymbol{h}_{\mathrm{B},l}\|\,\|\boldsymbol{h}_{\mathrm{B},l'}\|} \to 0,\ \forall l \neq l', \tag{10}$$

$$\frac{\boldsymbol{h}_{\mathrm{E},l}^\mathrm{H}\boldsymbol{h}_{\mathrm{E},l'}}{\|\boldsymbol{h}_{\mathrm{E},l}\|\,\|\boldsymbol{h}_{\mathrm{E},l'}\|} \to 0,\ \forall l \neq l', \tag{11}$$

$$\frac{\boldsymbol{h}_{\mathrm{B},l}^\mathrm{H}\boldsymbol{h}_{\mathrm{E},l'}}{\|\boldsymbol{h}_{\mathrm{B},l}\|\,\|\boldsymbol{h}_{\mathrm{E},l'}\|} \to 0. \tag{12}$$

It is worth mentioning that similar results have been developed in a previous paper (Lu and Zeng, 2023) for far-field communications, while requiring that different multipaths correspond to distinct AoDs.

Furthermore, by applying the simple path-based MRT beamforming with $\boldsymbol{f}_l = \sqrt{p_l}\boldsymbol{h}_{\mathrm{B},l}/\|\boldsymbol{h}_{\mathrm{B},l}\|$, where p_l denotes the power allocation of multipath l, the received signal at Bob is reduced to the following (Lu and Zeng, 2023):

$$y_\mathrm{B}[n] \to \left(\sum_{l=1}^{L_\mathrm{B}} \sqrt{p_l}\,\|\boldsymbol{h}_{\mathrm{B},l}\|\right) s[n - n_{\mathrm{B},\max}] + z_\mathrm{B}[n]. \tag{13}$$

Compared to the original received signal in Eq. (7), which is disrupted by ISI, the received signal in Eq. (13) achieves an ISI-free communication; i.e., the original time-dispersive channel has been transformed into an ISI-free AWGN channel, while making full use of all the L_B multipath signal components. The received signal-to-noise ratio (SNR) is given by

$$\gamma_\mathrm{B} = \frac{1}{\sigma^2}\left|\sum_{l=1}^{L_\mathrm{B}} \sqrt{p_l}\,\|\boldsymbol{h}_{\mathrm{B},l}\|\right|^2. \tag{14}$$

On the other hand, with the asymptotically orthogonal property in Eq. (12), when the scatterers experienced by Eve are different from those experienced by Bob, the received signal of Eve is approximated as

$$y_\mathrm{E}[n] \to z_\mathrm{E}[n], \tag{15}$$

which implies that no useful information is leaked to Eve, i.e., $\gamma_\mathrm{E} = 0$, without the need of the dedicated security-oriented beamforming design. As such, DAM enables an ISI-free and information leakage-free communication with delay precompensation and low-complexity path-based MRT beamforming.

The achievable secrecy rate in $\mathrm{b}/(\mathrm{s}\cdot\mathrm{Hz})$ is given by

$$\begin{aligned} R_\mathrm{sec} &= [\log_2(1+\gamma_\mathrm{B}) - \log_2(1+\gamma_\mathrm{E})]^+ \\ &= \log_2(1+\gamma_\mathrm{B}) \\ &= \log_2\left(1 + \frac{1}{\sigma^2}\left|\sum\nolimits_{l=1}^{L_\mathrm{B}} \sqrt{p_l}\,\|\boldsymbol{h}_{\mathrm{B},l}\|\right|^2\right), \end{aligned} \tag{16}$$

where $[x]^+ \triangleq \max(x, 0)$. Moreover, with the power constraint $\sum_{l=1}^{L_\mathrm{B}} p_l \le P$, the optimal power allocation $\{p_l\}_{l=1}^{L_\mathrm{B}}$ to maximize the secrecy rate in Eq. (16) can be obtained based on the Cauchy–Schwarz inequality, given by the following expression (Lu et al., 2024a):

$$p_l^\star = P\frac{\|\boldsymbol{h}_{\mathrm{B},l}\|^2}{\sum_{k=1}^{L_\mathrm{B}}\|\boldsymbol{h}_{\mathrm{B},k}\|^2},\ \forall l \in \{1, 2, \ldots, L_\mathrm{B}\}, \tag{17}$$

and the maximum achievable secrecy rate is

$$R_\mathrm{sec}^\star = \log_2\left(1 + \bar{P}\sum\nolimits_{l=1}^{L_\mathrm{B}}\|\boldsymbol{h}_{\mathrm{B},l}\|^2\right), \tag{18}$$

where $\bar{P} \triangleq P/\sigma^2$.

It is worth mentioning that due to the super-spatial resolution brought by XL-ULA, DAM can also enable ISI-free and information leakage-free communication when Eve is equipped with an antenna array; the details are omitted for brevity.

3.2 Path-based ZF beamforming toward ISI-free communication

In this subsection, path-based ZF beamforming is designed toward an ISI-free communication at

Bob, without the need of $M \gg L_{\mathrm{B}}$ and $M \gg L_{\mathrm{E}}$ as in the previous subsection.

A closer look at Eq. (7) shows that ISI can be completely eliminated by designing the path-based ZF beamforming as follows:

$$\boldsymbol{h}_{\mathrm{B},l}^{\mathrm{H}} \boldsymbol{f}_{l'} = 0,\ \forall l \neq l'. \tag{19}$$

Let $\boldsymbol{H}_{\mathrm{B},l} \in \mathbb{C}^{M\times(L_{\mathrm{B}}-1)} \triangleq [\boldsymbol{h}_{\mathrm{B},1}, \cdots, \boldsymbol{h}_{\mathrm{B},l-1}, \boldsymbol{h}_{\mathrm{B},l+1}, \cdots, \boldsymbol{h}_{\mathrm{B},L_{\mathrm{B}}}]$; the path-based ZF constraints in Eq. (19) can be compactly written as $\boldsymbol{H}_{\mathrm{B},l}^{\mathrm{H}} \boldsymbol{f}_l = \boldsymbol{0}_{(L_{\mathrm{B}}-1)\times 1},\ \forall l \in \{1,2,\ldots,L_{\mathrm{B}}\}$, which is feasible almost surely as long as $M \geq L_{\mathrm{B}}$. Moreover, let $\boldsymbol{H}_{\mathrm{B},l}^{\perp} \in \mathbb{C}^{M\times r_l}$ represent an orthonormal basis for the orthogonal complement of $\boldsymbol{H}_{\mathrm{B},l}$, with $r_l = \mathrm{rank}(\boldsymbol{H}_{\mathrm{B},l}^{\perp}) = M - L_{\mathrm{B}} + 1$. The path-based beamforming $\boldsymbol{f}_l$ satisfying Eq. (19) can be expressed as $\boldsymbol{f}_l = \boldsymbol{H}_{\mathrm{B},l}^{\perp} \boldsymbol{b}_l$, with $\boldsymbol{b}_l \in \mathbb{C}^{r_l\times 1}$ being the new vector to be designed (Lu and Zeng, 2022a). In this case, the received signal at Bob reduces to

$$y_{\mathrm{B}}[n] = \left(\sum_{l=1}^{L_{\mathrm{B}}} \boldsymbol{h}_{\mathrm{B},l}^{\mathrm{H}} \boldsymbol{H}_{\mathrm{B},l}^{\perp} \boldsymbol{b}_l\right) s[n - n_{\mathrm{B,max}}] + z_{\mathrm{B}}[n]. \tag{20}$$

Similar to Eq. (13), the time-dispersive channel is transformed into the ISI-free AWGN channel, and the received SNR is

$$\gamma_{\mathrm{B}} = \frac{1}{\sigma^2}\left|\sum_{l=1}^{L_{\mathrm{B}}} \boldsymbol{h}_{\mathrm{B},l}^{\mathrm{H}} \boldsymbol{H}_{\mathrm{B},l}^{\perp} \boldsymbol{b}_l\right|^2. \tag{21}$$

Note that such a path-based ZF DAM beamforming achieves a dual function. On one hand, it completely eliminates ISI issue at Bob. On the other hand, without requiring CSI of Eve, the transmit signal of DAM in fact introduces ISI to Eve, as becomes clearer later. This achieves a similar effect as the dedicated AN, whereas DAM does not cost the precious transmit power.

It is worth mentioning that the symbols in the received signal at Eve, i.e., Eq. (8), may have an identical delay difference. To derive the signal-to-interference-plus-noise ratio (SINR) of Eve, these symbols should be properly grouped (Zeng et al., 2018). Specifically, the delay difference $\Delta_{\mathrm{B}l',\mathrm{E}l}$ satisfies $\Delta_{\mathrm{B}l',\mathrm{E}l} \in [\Delta_{\mathrm{BE,min}}, \Delta_{\mathrm{BE,max}}]$, where $\Delta_{\mathrm{BE,min}} = n_{\mathrm{B,min}} - n_{\mathrm{E,max}}$ and $\Delta_{\mathrm{BE,max}} = n_{\mathrm{B,max}} - n_{\mathrm{E,min}}$. Then, for any delay difference $i \in [\Delta_{\mathrm{BE,min}}, \Delta_{\mathrm{BE,max}}]$, we define the following effective channel:

$$\boldsymbol{g}_{\mathrm{E},l'}[i] = \begin{cases} \boldsymbol{h}_{\mathrm{E},l}, & \text{if } \exists l \in \{1,2,\ldots,L_{\mathrm{E}}\} \text{ s.t. } \Delta_{\mathrm{B}l',\mathrm{E}l} = i, \\ \boldsymbol{0}, & \text{otherwise.} \end{cases} \tag{22}$$

Let $i^\star = \underset{\Delta_{\mathrm{BE,min}} \leq i \leq \Delta_{\mathrm{BE,max}}}{\arg\max} \sum_{l'=1}^{L_{\mathrm{B}}} \|\boldsymbol{g}_{\mathrm{E},l'}[i]\|^2$; the received signal of Eve in Eq. (8) can be equivalently written as

$$\begin{aligned} y_{\mathrm{E}}[n] = &\left(\sum_{l'=1}^{L_{\mathrm{B}}} \boldsymbol{g}_{\mathrm{E},l'}^{\mathrm{H}}[i^\star] \boldsymbol{f}_{l'}\right) s[n - n_{\mathrm{B,max}} + i^\star] \\ &+ \sum_{i=\Delta_{\mathrm{BE,min}}, i\neq i^\star}^{\Delta_{\mathrm{BE,max}}} \left(\sum_{l'=1}^{L_{\mathrm{B}}} \boldsymbol{g}_{\mathrm{E},l'}^{\mathrm{H}}[i] \boldsymbol{f}_{l'}\right) \\ &\cdot s[n - n_{\mathrm{B,max}} + i] + z_{\mathrm{E}}[n]. \end{aligned} \tag{23}$$

Thus, the received SINR at Eve is

$$\gamma_{\mathrm{E}} = \frac{\left|\sum_{l'=1}^{L_{\mathrm{B}}} \boldsymbol{g}_{\mathrm{E},l'}^{\mathrm{H}}[i^\star] \boldsymbol{f}_{l'}\right|^2}{\sum_{i=\Delta_{\mathrm{BE,min}}, i\neq i^\star}^{\Delta_{\mathrm{BE,max}}} \left|\sum_{l'=1}^{L_{\mathrm{B}}} \boldsymbol{g}_{\mathrm{E},l'}^{\mathrm{H}}[i] \boldsymbol{f}_{l'}\right|^2 + \sigma^2}. \tag{24}$$

The received SNR of Bob in Eq. (21) is maximized by optimizing the new beamforming vector $\{\boldsymbol{b}_l\}_{l=1}^{L_{\mathrm{B}}}$, while ignoring the received SINR of Eve. The problem can be formulated as follows:

$$\max_{\{\boldsymbol{b}_l\}_{l=1}^{L_{\mathrm{B}}}} \frac{1}{\sigma^2}\left|\sum_{l=1}^{L_{\mathrm{B}}} \boldsymbol{h}_{\mathrm{B},l}^{\mathrm{H}} \boldsymbol{H}_{\mathrm{B},l}^{\perp} \boldsymbol{b}_l\right|^2 \text{ s.t. } \sum_{l=1}^{L_{\mathrm{B}}} \left\|\boldsymbol{H}_{\mathrm{B},l}^{\perp} \boldsymbol{b}_l\right\|^2 \leq P. \tag{25}$$

Similarly, according to the Cauchy–Schwarz inequality, the optimal path-based ZF beamforming is (Lu and Zeng, 2023)

$$\boldsymbol{f}_l^{\mathrm{ZF}} = \frac{\sqrt{P}\boldsymbol{H}_{\mathrm{B},l}^{\perp}\left(\boldsymbol{H}_{\mathrm{B},l}^{\perp}\right)^{\mathrm{H}} \boldsymbol{h}_{\mathrm{B},l}}{\sqrt{\sum_{k=1}^{L_{\mathrm{B}}} \left\|\left(\boldsymbol{H}_{\mathrm{B},k}^{\perp}\right)^{\mathrm{H}} \boldsymbol{h}_{\mathrm{B},k}\right\|^2}}, \tag{26}$$

and the corresponding SNR is

$$\gamma_{\mathrm{B}}^{\mathrm{ZF}} = \bar{P} \sum_{l=1}^{L_{\mathrm{B}}} \left\|\left(\boldsymbol{H}_{\mathrm{B},l}^{\perp}\right)^{\mathrm{H}} \boldsymbol{h}_{\mathrm{B},l}\right\|^2. \tag{27}$$

By substituting Eq. (26) into Eq. (24), the received SINR of Eve is then obtained, denoted as $\gamma_{\mathrm{E}}^{\mathrm{ZF}}$. Let $n_{\mathrm{c}} \approx T_{\mathrm{c}}/T_{\mathrm{s}}$ denote the number of symbol samples within each channel coherence block, where T_{c} denotes the channel coherence time and $T_{\mathrm{s}} = 1/B$ with

B being the system bandwidth. It is worth mentioning that the received signal of Bob in Eq. (7) is at the most delayed by $n_{\mathrm{B,max}}+n_{\mathrm{B,max}}-n_{\mathrm{B,min}} \approx 2n_{\mathrm{B,max}}$. To circumvent ISI across consecutive channel coherence blocks, a guard interval of length $2\tilde{n}_{\mathrm{B,max}}$ is required at the beginning of each channel coherence block; i.e., the guard interval overhead of DAM transmission is $2n_{\mathrm{B,max}}/n_{\mathrm{c}}$. Thus, the effective achievable secrecy rate in this case is

$$R_{\mathrm{sec}}^{\mathrm{ZF}} = \frac{n_{\mathrm{c}}-2n_{\mathrm{B,max}}}{n_{\mathrm{c}}}\left[\log_2\left(1+\gamma_{\mathrm{B}}^{\mathrm{ZF}}\right) - \log_2\left(1+\gamma_{\mathrm{E}}^{\mathrm{ZF}}\right)\right]^+. \tag{28}$$

Note that the main complexity of obtaining the path-based ZF beamforming vectors lies in calculating the orthogonal complement, which has the complexity of $\mathcal{O}\left(ML_{\mathrm{B}}(L_{\mathrm{B}}-1)^2\right)$.

4 Path-based optimized DAM beamforming

In this section, we consider the general case in the presence of some tolerable ISI, instead of completely eliminating ISI. In this case, the path-based beamforming is optimized to maximize the secrecy rate.

To reveal the fundamental performance limit of DAM, CSI of Eve is assumed to be available at Alice. Similar to Eq. (24), to derive SINR of Bob, the received signal of Bob in Eq. (7) can be equivalently written as

$$\begin{aligned} y_{\mathrm{B}}[n] = &\left(\sum_{l=1}^{L_{\mathrm{B}}} \boldsymbol{h}_{\mathrm{B},l}^{\mathrm{H}}\boldsymbol{f}_l\right) s\left[n-n_{\mathrm{B,max}}\right] \\ &+ \sum_{i=\Delta_{\mathrm{BB,min}},i\neq 0}^{\Delta_{\mathrm{BB,max}}} \left(\sum_{l'=1}^{L_{\mathrm{B}}} \boldsymbol{g}_{\mathrm{B},l'}^{\mathrm{H}}[i]\,\boldsymbol{f}_{l'}\right) \\ &\cdot s\left[n-n_{\mathrm{B,max}}+i\right]+z_{\mathrm{B}}[n], \end{aligned} \tag{29}$$

where $\Delta_{\mathrm{BB,min}}$, $\Delta_{\mathrm{BB,max}}$, and $\boldsymbol{g}_{\mathrm{B},l'}[i]$ follow the similar definitions as $\Delta_{\mathrm{BE,min}}$, $\Delta_{\mathrm{BE,max}}$, and $\boldsymbol{g}_{\mathrm{E},l'}[i]$, respectively. The received SINR of Bob is

$$\begin{aligned} \gamma_{\mathrm{B}} &= \frac{\left|\sum_{l=1}^{L_{\mathrm{B}}} \boldsymbol{h}_{\mathrm{B},l}^{\mathrm{H}}\boldsymbol{f}_l\right|^2}{\sum_{i=\Delta_{\mathrm{BB,min}},i\neq 0}^{\Delta_{\mathrm{BB,max}}} \left|\sum_{l'=1}^{L_{\mathrm{B}}} \boldsymbol{g}_{\mathrm{B},l'}^{\mathrm{H}}[i]\,\boldsymbol{f}_{l'}\right|^2+\sigma^2} \\ &= \frac{\bar{\boldsymbol{f}}^{\mathrm{H}}\bar{\boldsymbol{h}}_{\mathrm{B}}\bar{\boldsymbol{h}}_{\mathrm{B}}^{\mathrm{H}}\bar{\boldsymbol{f}}}{\bar{\boldsymbol{f}}^{\mathrm{H}}\left(\sum_{i=\Delta_{\mathrm{BB,min}},i\neq 0}^{\Delta_{\mathrm{BB,max}}} \bar{\boldsymbol{g}}_{\mathrm{B}}[i]\,\bar{\boldsymbol{g}}_{\mathrm{B}}^{\mathrm{H}}[i]\right)\bar{\boldsymbol{f}}+\sigma^2} \\ &= \frac{\bar{\boldsymbol{f}}^{\mathrm{H}}\boldsymbol{A}\bar{\boldsymbol{f}}}{\bar{\boldsymbol{f}}^{\mathrm{H}}\boldsymbol{B}\bar{\boldsymbol{f}}+1}, \end{aligned} \tag{30}$$

where $\bar{\boldsymbol{h}}_{\mathrm{B}} \in \mathbb{C}^{ML_{\mathrm{B}}\times 1} \triangleq [\boldsymbol{h}_{\mathrm{B},1}^{\mathrm{T}}, \boldsymbol{h}_{\mathrm{B},2}^{\mathrm{T}}, \cdots, \boldsymbol{h}_{\mathrm{B},L_{\mathrm{B}}}^{\mathrm{T}}]^{\mathrm{T}}$, $\bar{\boldsymbol{f}} \in \mathbb{C}^{ML_{\mathrm{B}}\times 1} \triangleq [\boldsymbol{f}_1^{\mathrm{T}}, \boldsymbol{f}_2^{\mathrm{T}}, \cdots, \boldsymbol{f}_{L_{\mathrm{B}}}^{\mathrm{T}}]^{\mathrm{T}}$, $\bar{\boldsymbol{g}}_{\mathrm{B}}[i] \in \mathbb{C}^{ML_{\mathrm{B}}\times 1} \triangleq [\boldsymbol{g}_{\mathrm{B},1}^{\mathrm{T}}[i], \boldsymbol{g}_{\mathrm{B},2}^{\mathrm{T}}[i], \cdots, \boldsymbol{g}_{\mathrm{B},L_{\mathrm{B}}}^{\mathrm{T}}[i]]^{\mathrm{T}}$, $\boldsymbol{A} \in \mathbb{C}^{(ML_{\mathrm{B}})\times(ML_{\mathrm{B}})} \triangleq \frac{1}{\sigma^2}\bar{\boldsymbol{h}}_{\mathrm{B}}\bar{\boldsymbol{h}}_{\mathrm{B}}^{\mathrm{H}}$, and $\boldsymbol{B} \in \mathbb{C}^{(ML_{\mathrm{B}})\times(ML_{\mathrm{B}})} \triangleq \sum_{i=\Delta_{\mathrm{BB,min}},i\neq 0}^{\Delta_{\mathrm{BB,max}}} \frac{1}{\sigma^2}\bar{\boldsymbol{g}}_{\mathrm{B}}[i]\,\bar{\boldsymbol{g}}_{\mathrm{B}}^{\mathrm{H}}[i]$.

In addition, let $\bar{\boldsymbol{g}}_{\mathrm{E}}[i] \in \mathbb{C}^{ML_{\mathrm{B}}\times 1} \triangleq [\boldsymbol{g}_{\mathrm{E},1}^{\mathrm{T}}[i], \boldsymbol{g}_{\mathrm{E},2}^{\mathrm{T}}[i], \cdots, \boldsymbol{g}_{\mathrm{E},L_{\mathrm{B}}}^{\mathrm{T}}[i]]^{\mathrm{T}}$. The received SINR of Eve in Eq. (24) can be expressed as

$$\begin{aligned} \gamma_{\mathrm{E}} &= \frac{\bar{\boldsymbol{f}}^{\mathrm{H}}\bar{\boldsymbol{g}}_{\mathrm{E}}[i^\star]\,\bar{\boldsymbol{g}}_{\mathrm{E}}^{\mathrm{H}}[i^\star]\,\bar{\boldsymbol{f}}}{\bar{\boldsymbol{f}}^{\mathrm{H}}\left(\sum_{i=\Delta_{\mathrm{BE,min}},i\neq i^\star}^{\Delta_{\mathrm{BE,max}}} \bar{\boldsymbol{g}}_{\mathrm{E}}[i]\,\bar{\boldsymbol{g}}_{\mathrm{E}}^{\mathrm{H}}[i]\right)\bar{\boldsymbol{f}}+\sigma^2} \\ &= \frac{\bar{\boldsymbol{f}}^{\mathrm{H}}\boldsymbol{C}\bar{\boldsymbol{f}}}{\bar{\boldsymbol{f}}^{\mathrm{H}}\boldsymbol{D}\bar{\boldsymbol{f}}+1}, \end{aligned} \tag{31}$$

where $\boldsymbol{C} \in \mathbb{C}^{(ML_{\mathrm{B}})\times(ML_{\mathrm{B}})} \triangleq \frac{1}{\sigma^2}\bar{\boldsymbol{g}}_{\mathrm{E}}[i^\star]\,\bar{\boldsymbol{g}}_{\mathrm{E}}^{\mathrm{H}}[i^\star]$ and $\boldsymbol{D} \in \mathbb{C}^{(ML_{\mathrm{B}})\times(ML_{\mathrm{B}})} \triangleq \sum_{i=\Delta_{\mathrm{BE,min}},i\neq i^\star}^{\Delta_{\mathrm{BE,max}}} \frac{1}{\sigma^2}\bar{\boldsymbol{g}}_{\mathrm{E}}[i]\,\bar{\boldsymbol{g}}_{\mathrm{E}}^{\mathrm{H}}[i]$.

The secrecy rate can be maximized by optimizing the beamforming vector $\bar{\boldsymbol{f}}$, which can be formulated as

$$\begin{aligned} &\max_{\bar{\boldsymbol{f}}} \left(\log_2\left(1+\frac{\bar{\boldsymbol{f}}^{\mathrm{H}}\boldsymbol{A}\bar{\boldsymbol{f}}}{\bar{\boldsymbol{f}}^{\mathrm{H}}\boldsymbol{B}\bar{\boldsymbol{f}}+1}\right)-\log_2\left(1+\frac{\bar{\boldsymbol{f}}^{\mathrm{H}}\boldsymbol{C}\bar{\boldsymbol{f}}}{\bar{\boldsymbol{f}}^{\mathrm{H}}\boldsymbol{D}\bar{\boldsymbol{f}}+1}\right)\right) \\ &\text{s.t. } \left\|\bar{\boldsymbol{f}}\right\|^2 \leq P. \end{aligned} \tag{32}$$

It is worth mentioning that the optimal value of problem (32) is nonnegative, since if $R_{\mathrm{sec}} < 0$, the beamforming vector can be set as $\bar{\boldsymbol{f}} = \boldsymbol{0}$ such that $R_{\mathrm{sec}} = 0$. Moreover, the non-concave objective function renders problem (32) difficult to be directly solved. To solve problem (32), the objective function is expressed as

$$\begin{aligned} &\log_2\left(\bar{\boldsymbol{f}}^{\mathrm{H}}(\boldsymbol{A}+\boldsymbol{B})\,\bar{\boldsymbol{f}}+1\right)-\log_2\left(\bar{\boldsymbol{f}}^{\mathrm{H}}\boldsymbol{B}\bar{\boldsymbol{f}}+1\right) \\ &-\log_2\left(\bar{\boldsymbol{f}}^{\mathrm{H}}(\boldsymbol{C}+\boldsymbol{D})\,\bar{\boldsymbol{f}}+1\right)+\log_2\left(\bar{\boldsymbol{f}}^{\mathrm{H}}\boldsymbol{D}\bar{\boldsymbol{f}}+1\right). \end{aligned} \tag{33}$$

The auxiliary variable $\boldsymbol{t}=[t_1,t_2,t_3,t_4]^{\mathrm{T}}$ is then introduced such that

$$\log_2\left(\bar{\boldsymbol{f}}^{\mathrm{H}}(\boldsymbol{A}+\boldsymbol{B})\bar{\boldsymbol{f}}+1\right)\geq t_1, \tag{34a}$$
$$\log_2\left(\bar{\boldsymbol{f}}^{\mathrm{H}}\boldsymbol{B}\bar{\boldsymbol{f}}+1\right)\leq t_2, \tag{34b}$$
$$\log_2\left(\bar{\boldsymbol{f}}^{\mathrm{H}}(\boldsymbol{C}+\boldsymbol{D})\bar{\boldsymbol{f}}+1\right)\leq t_3, \tag{34c}$$
$$\log_2\left(\bar{\boldsymbol{f}}^{\mathrm{H}}\boldsymbol{D}\bar{\boldsymbol{f}}+1\right)\geq t_4. \tag{34d}$$

Thus, problem (32) is equivalently written as

$$\max_{\bar{\boldsymbol{f}},\boldsymbol{t}}(t_1-t_2-t_3+t_4)\ \text{s.t.}\ \left\|\bar{\boldsymbol{f}}\right\|^2\leq P,\ \text{constraints (34)}. \tag{35}$$

To tackle the non-convex constraints (34), the auxiliary variable $\boldsymbol{q}=[q_1,q_2,q_3,q_4]^{\mathrm{T}}$ is further introduced such that

$$\log_2 q_1\geq t_1, \tag{36a}$$
$$\bar{\boldsymbol{f}}^{\mathrm{H}}(\boldsymbol{A}+\boldsymbol{B})\bar{\boldsymbol{f}}+1\geq q_1, \tag{36b}$$
$$\log_2 q_2\leq t_2, \tag{36c}$$
$$\bar{\boldsymbol{f}}^{\mathrm{H}}\boldsymbol{B}\bar{\boldsymbol{f}}+1\leq q_2, \tag{36d}$$
$$\log_2 q_3\leq t_3, \tag{36e}$$
$$\bar{\boldsymbol{f}}^{\mathrm{H}}(\boldsymbol{C}+\boldsymbol{D})\bar{\boldsymbol{f}}+1\leq q_3, \tag{36f}$$
$$\log_2 q_4\geq t_4, \tag{36g}$$
$$\bar{\boldsymbol{f}}^{\mathrm{H}}\boldsymbol{D}\bar{\boldsymbol{f}}+1\geq q_4. \tag{36h}$$

A closer look at constraints (36) shows that constraints (36a), (36d), (36f), and (36g) are convex, while the remaining constraints are non-convex. Fortunately, the SCA technique can be used to effectively address this issue (Zeng et al., 2019). Specifically, let $\bar{\boldsymbol{f}}^{(k)}$, $q_2^{(k)}$, and $q_3^{(k)}$ denote the resulting optimization variables after the k^{th} iteration. We have

$$\begin{aligned}&\left(\bar{\boldsymbol{f}}^{(k)}\right)^{\mathrm{H}}(\boldsymbol{A}+\boldsymbol{B})\bar{\boldsymbol{f}}^{(k)}\\&+2\mathrm{Re}\left\{\left(\bar{\boldsymbol{f}}-\bar{\boldsymbol{f}}^{(k)}\right)^{\mathrm{H}}(\boldsymbol{A}+\boldsymbol{B})\bar{\boldsymbol{f}}^{(k)}\right\}+1\geq q_1,\end{aligned} \tag{37a}$$
$$\log_2 q_2^{(k)}+\frac{q_2-q_2^{(k)}}{q_2^{(k)}\ln 2}\leq t_2, \tag{37b}$$
$$\log_2 q_3^{(k)}+\frac{q_3-q_3^{(k)}}{q_3^{(k)}\ln 2}\leq t_3, \tag{37c}$$
$$\begin{aligned}&\left(\bar{\boldsymbol{f}}^{(k)}\right)^{\mathrm{H}}\boldsymbol{D}\bar{\boldsymbol{f}}^{(k)}\\&+2\mathrm{Re}\left\{\left(\bar{\boldsymbol{f}}-\bar{\boldsymbol{f}}^{(k)}\right)^{\mathrm{H}}\boldsymbol{D}\bar{\boldsymbol{f}}^{(k)}\right\}+1\geq q_4.\end{aligned} \tag{37d}$$

As a result, problem (32) can be transformed into

$$\begin{aligned}&\max_{\bar{\boldsymbol{f}},\boldsymbol{t},\boldsymbol{q}}\ (t_1-t_2-t_3+t_4)\\&\text{s.t.}\ \left\|\bar{\boldsymbol{f}}\right\|^2\leq P,\\&\quad\text{constraints (36a), (36d), (36f), (36g),}\\&\quad\text{(37a), (37b), (37c), (37d),}\end{aligned} \tag{38}$$

which is a convex problem and can be solved via the standard convex optimization tools, such as CVX. The complexity for obtaining the path-based optimized DAM beamforming is approximately $\mathcal{O}\left(I(ML_{\mathrm{B}})^3\right)$, with I denoting the number of iterations.

5 Benchmarking scheme: AN-based OFDM

In this section, as a comparison, the benchmarking scheme of AN-based OFDM is considered, which can deteriorate the eavesdropping channel without requiring CSI of Eve. Let K denote the number of subcarriers. The channel frequency response of the k^{th} subcarrier is

$$\boldsymbol{h}_a[k]=\frac{1}{\sqrt{K}}\sum_{l=1}^{L_a}\boldsymbol{h}_{a,l}\mathrm{e}^{-\mathrm{j}\frac{2\pi k n_{al}}{K}},\ 0\leq k\leq K-1, \tag{39}$$

where $a\in\{\mathrm{B},\mathrm{E}\}$. Let p_k denote the transmit power of the k^{th} subcarrier, and η denote the fraction of power allocated to the information-bearing symbol. The remaining fraction of power is allocated to the AN, which is transmitted in all the directions except toward Bob (Zhou XY and McKay, 2010; Romero-Zurita et al., 2011). For subcarrier k, let $\bar{\boldsymbol{F}}_k=[\boldsymbol{f}_k,\boldsymbol{F}_k]$ be an orthonormal basis of an M-dimensional space, where $\boldsymbol{f}_k=\boldsymbol{h}_{\mathrm{B}}[k]/\left\|\boldsymbol{h}_{\mathrm{B}}[k]\right\|$. The transmitted signal of the AN-based OFDM scheme is

$$\boldsymbol{x}[k]=\sqrt{p_k\eta}\boldsymbol{f}_k s[k]+\sqrt{p_k(1-\eta)}\boldsymbol{F}_k\boldsymbol{w}[k], \tag{40}$$

where $\boldsymbol{f}_k\in\mathbb{C}^{M\times 1}$ denotes the frequency-domain beamforming of subcarrier k, $s[k]$ denotes the information-bearing symbol of subcarrier k, with $\mathbb{E}[|s[k]|^2]=1$, and $\boldsymbol{w}[k]\in\mathbb{C}^{(M-1)\times 1}$ denotes the AN vector, with $\mathbb{E}\left[\boldsymbol{w}[k]\boldsymbol{w}^{\mathrm{H}}[k]\right]=\boldsymbol{I}/(M-1)$ and $\boldsymbol{I}$ being the identity matrix.

After removing the cyclic prefix (CP), the

received frequency-domain signal at Bob is

$$\begin{aligned} y_{\mathrm{B}}[k] &= \boldsymbol{h}_{\mathrm{B}}^{\mathrm{H}}[k]\,\boldsymbol{x}[k] + z_{\mathrm{B}}[k] \\ &= \sqrt{p_k \eta}\,\|\boldsymbol{h}_{\mathrm{B}}[k]\|\,s[k] + z_{\mathrm{B}}[k]. \end{aligned} \tag{41}$$

It is observed that Bob is free from the impact of AN, and the received SNR is

$$\gamma_{\mathrm{B}}[k] = \frac{p_k \eta \|\boldsymbol{h}_{\mathrm{B}}[k]\|^2}{\sigma^2}, \tag{42}$$

where the transmit power of each subcarrier can be obtained via the classic water-filling algorithm (Goldsmith, 2005). In addition, the received frequency-domain signal at Eve is

$$\begin{aligned} y_{\mathrm{E}}[k] =& \boldsymbol{h}_{\mathrm{E}}^{\mathrm{H}}[k]\,\boldsymbol{x}[k] + z_{\mathrm{E}}[k] \\ =& \sqrt{p_k \eta}\frac{\boldsymbol{h}_{\mathrm{E}}^{\mathrm{H}}[k]\,\boldsymbol{h}_{\mathrm{B}}[k]}{\|\boldsymbol{h}_{\mathrm{B}}[k]\|}s[k] \\ &+ \sqrt{p_k(1-\eta)}\boldsymbol{h}_{\mathrm{E}}^{\mathrm{H}}[k]\,\boldsymbol{F}_k \boldsymbol{w}[k] + z_{\mathrm{E}}[k]. \end{aligned} \tag{43}$$

Due to the interference of AN, the received SINR of Eve is

$$\gamma_{\mathrm{E}}[k] = \frac{\frac{p_k \eta}{\|\boldsymbol{h}_{\mathrm{B}}[k]\|^2}\left|\boldsymbol{h}_{\mathrm{E}}^{\mathrm{H}}[k]\,\boldsymbol{h}_{\mathrm{B}}[k]\right|^2}{\frac{p_k(1-\eta)}{M-1}\left\|\boldsymbol{F}_k^{\mathrm{H}}\boldsymbol{h}_{\mathrm{E}}[k]\right\|^2 + \sigma^2}. \tag{44}$$

Let n_{CP} denote the length of CP. The achievable secrecy rate of AN-based OFDM scheme is

$$\begin{aligned} R_{\mathrm{sec}} =& \frac{1}{K+n_{\mathrm{CP}}}\sum_{k=0}^{K-1}\left[\log_2(1+\gamma_{\mathrm{B}}[k])\right. \\ &\left. - \log(1+\gamma_{\mathrm{E}}[k])\right]^+, \end{aligned} \tag{45}$$

and the optimal power allocation coefficient η to maximize Eq. (45) can be efficiently obtained by a one-dimensional search.

6 Simulation results

In this section, simulation results are presented to verify the performance of DAM secure transmission. We consider an mmWave system operating at $f = 28$ GHz, with its system bandwidth given by $B = 128$ MHz. The noise power spectrum density is -174 dBm/Hz, and the transmit power is set as $P = 40$ dBm. Under a two-dimensional Cartesian coordinate system, Alice is equipped with a ULA, which is placed along the y axis and centered at the origin. The locations of Alice, Bob, and Eve are $[0\text{ m}, 0\text{ m}]$, $[75\text{ m}, 0\text{ m}]$, and $[70\text{ m}, -5\text{ m}]$, respectively. The numbers of multipaths for Bob and Eve are $L_{\mathrm{B}} = L_{\mathrm{E}} = 5$, with the corresponding scatterers uniformly distributed in the region $r_l \in [30\text{ m}, 70\text{ m}]$ and $\theta_l \in [-60°, 60°]$. In addition, the complex-valued gain of each multipath is generated based on the model developed in a previous work (Dong ZJ and Zeng, 2022). The channel coherence time is $T_{\mathrm{c}} = 1$ ms, and the upper bound of the maximum delay of Bob is $\tilde{n}_{\mathrm{B,max}} = n_{\mathrm{B,max}} = 75$. For the benchmarking scheme of AN-based OFDM, the number of subcarriers is $K = 512$, and the CP length is chosen as $n_{\mathrm{CP}} = 75$.

Fig. 3 shows the secrecy rate versus the number of antenna elements M for the DAM transmission and AN-based OFDM schemes. The transmit power of Alice is $P = 40$ dBm. It is observed that as the antenna number M increases, path-based ZF beamforming yields a comparable performance to path-based optimized beamforming, which is expected, since for a large M, both the beamforming schemes are able to well distinguish all multipath signal components of Bob and Eve. It is also observed that compared to the AN-based OFDM scheme, the two DAM beamforming schemes achieve considerable gain, which is due to the following two reasons: on one hand, compared to the OFDM scheme that inserts a CP at each OFDM symbol, DAM is able to significantly reduce the guard interval overhead. Specifically, the guard interval overhead of DAM secure transmission is $2\tilde{n}_{\mathrm{B,max}}/n_{\mathrm{c}} = \frac{2\times 75}{1.28\times 10^5} = 0.12\%$. By contrast, CP overhead of AN-based OFDM is $n_{\mathrm{OFDM}} \times n_{\mathrm{CP}}/n_{\mathrm{c}} \approx n_{\mathrm{CP}}/(K+n_{\mathrm{CP}}) = 75/(512+75) = 12.8\%$. On the other hand, DAM secure transmission inherently introduces ISI to Eve, which saves the power allocating to the AN. This can be reflected

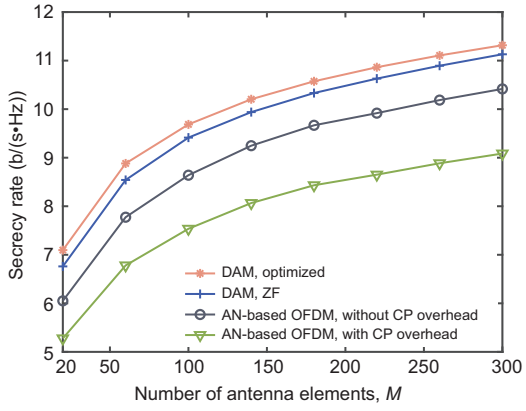

Fig. 3 Secrecy rate versus the number of antenna elements at Alice

by the observation that the DAM secure transmission is still superior to AN-based OFDM when the impact of CP overhead is excluded.

Furthermore, Fig. 4 compares the secrecy rate of near-field beamforming (NFB) and far-field beamforming (FFB) schemes. Specifically, the multipath channel vectors of $\{\boldsymbol{h}_{\mathrm{B},l}\}_{l=1}^{L_{\mathrm{B}}}$ and $\{\boldsymbol{h}_{\mathrm{E},l}\}_{l=1}^{L_{\mathrm{E}}}$ adopt the accurate near-field NUSW-based model, and the NFB and FFB schemes are designed based on the near-field NUSW- and far-field UPW-based channel models, respectively. As can be observed, for a relatively small antenna number M, the FFB schemes of DAM and AN-based OFDM achieve comparable secrecy rate as the near-field counterparts. The reason is that when M is relatively small, Bob/Eve/scatterers are located in the far-field region, where the far-field UPW model sufficiently well approximates the near-field NUSW model. Nevertheless, a further increase of M expands the near-field region, rendering the far-field UPW model inaccurate for the near-field channel. As such, the secrecy rate of the FFB schemes begins to deviate from that of NFB counterparts when M continues to increase, whether for DAM or for AN-based OFDM. The significant performance loss of FFB beamforming indicates that it is necessary to consider the NUSW model in the near-field region.

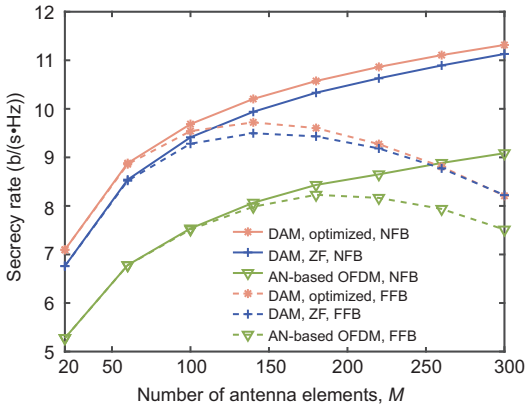

Fig. 4 Secrecy rate versus the number of antenna elements for near-field beamforming (NFB) and far-field beamforming (FFB)

Fig. 5 plots the complementary cumulative distribution function (CCDF) of PAPR for DAM and AN-based OFDM. The number of transmit antennas is $M = 256$, and 128QAM is considered (QAM is short for quadrature amplitude modulation). It is observed that the single-carrier DAM secure transmission achieves a more notable PAPR reduction than the AN-based OFDM, while simultaneously enhancing the secrecy rate, as shown in Fig. 3. This is because, as can be seen from Eq. (5), the transmitted signal of DAM is dependent on the number of multipaths L_{B}, implying that only L_{B} multipath signal components are mixed at each antenna. By contrast, the AN-based OFDM superposes $M \gg L_{\mathrm{B}}$ subcarrier signals at each antenna.

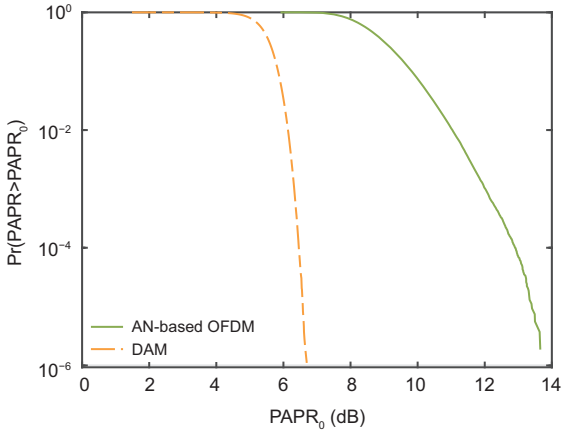

Fig. 5 Comparison of PAPR for DAM and AN-based OFDM

7 Conclusions

This paper investigated the near-field secure communication via DAM. Based on the near-field NUSW model, it was first shown that delay compensation and low-complexity path-based MRT beamforming asymptotically achieve an ISI-free and information leakage-free communication when the antenna number of Alice is much larger than the number of multipaths for Bob and Eve. Further, an ISI-free communication was obtained with path-based ZF beamforming, for which the secrecy rate was evaluated. Moreover, the secrecy rate was maximized by optimizing the path-based DAM beamforming under some tolerable ISI. For comparison, the benchmarking scheme of the AN-based OFDM was considered. Simulation results showed that the proposed DAM yields a better secrecy rate and PAPR performance than the AN-based OFDM scheme.

Despite the above-mentioned effectiveness, secure wireless communication with DAM still faces some challenges. For instance, the security robustness of DAM against sophisticated or unconventional

attacks requires more in-depth study in the future. Moreover, to avoid high energy consumption, low-resolution devices and antenna selection can be adopted, and energy-efficient secure communication with DAM is important to investigate in the future.

Contributors

Haiquan LU and Yong ZENG designed the research. Haiquan LU processed the data and drafted the paper. Yong ZENG helped organize the paper. Haiquan LU and Yong ZENG revised and finalized the paper.

Conflict of interest

Both the authors declare that they have no conflict of interest.

Data availability

The data that support the findings of this study are available from the corresponding author upon reasonable request.

References

Chen JG, Xiao Y, Liu KL, et al., 2024. Physical layer security for near-field communications via directional modulation. *IEEE Trans Veh Technol*, 73(8):12242-12246. https://doi.org/10.1109/TVT.2024.3382324

Cheng YJ, Huang CW, Peng W, et al., 2024. Achievable rate optimization of the RIS-aided near-field wideband uplink. *IEEE Trans Wirel Commun*, 23(3):2296-2311. https://doi.org/10.1109/TWC.2023.3297396

Cui M, Zhang GC, Zhang R, 2019. Secure wireless communication via intelligent reflecting surface. *IEEE Wirel Commun Lett*, 8(5):1410-1414. https://doi.org/10.1109/LWC.2019.2919685

Cui MY, Dai LL, 2022. Channel estimation for extremely large-scale MIMO: far-field or near-field? *IEEE Trans Commun*, 70(4):2663-2677. https://doi.org/10.1109/TCOMM.2022.3146400

Ding DY, Zeng Y, Wang DM, 2024. Channel estimation for delay alignment modulation. IEEE Wireless Communications and Networking Conf, p.1-6. https://doi.org/10.1109/WCNC57260.2024.10570876

Dong L, Han Z, Petropulu AP, et al., 2010. Improving wireless physical layer security via cooperating relays. *IEEE Trans Signal Process*, 58(3):1875-1888. https://doi.org/10.1109/TSP.2009.2038412

Dong ZJ, Zeng Y, 2022. Near-field spatial correlation for extremely large-scale array communications. *IEEE Commun Lett*, 26(7):1534-1538. https://doi.org/10.1109/LCOMM.2022.3170735

Ferreira J, Guerreiro J, Dinis R, 2024. Physical layer security with near-field beamforming. *IEEE Access*, 12:4801-4811. https://doi.org/10.1109/ACCESS.2023.3344654

Goldsmith A, 2005. Wireless Communications. Cambridge University Press, Cambridge, UK.

Gong TR, Wei L, Huang CW, et al., 2024. Holographic MIMO communications with arbitrary surface placements: near-field LoS channel model and capacity limit. *IEEE J Sel Areas Commun*, 42(6):1549-1566. https://doi.org/10.1109/JSAC.2024.3389126

Hao WM, Shi H, Sun GC, et al., 2023. Joint beamforming design for active RIS-aided THz ISAC systems with delay alignment modulation. *IEEE Wirel Commun Lett*, 12(10):1816-1820. https://doi.org/10.1109/LWC.2023.3295912

Hong T, Song MZ, Liu Y, 2011. Dual-beam directional modulation technique for physical-layer secure communication. *IEEE Antenn Wirel Propag Lett*, 10:1417-1420. https://doi.org/10.1109/LAWP.2011.2178384

Illi E, Qaraqe M, El Bouanani F, et al., 2024. Enhancing physical layer security with reconfigurable intelligent surfaces and friendly jamming: a secrecy analysis. *Comput Commun*, 221:106-119. https://doi.org/10.1016/j.comcom.2024.04.010

Li XR, Dong ZJ, Zeng Y, et al., 2024. Multi-user modular XL-MIMO communications: near-field beam focusing pattern and user grouping. *IEEE Trans Wirel Commun*, 23(10):13766-13781. https://doi.org/10.1109/TWC.2024.3404659

Liu Y, Xu K, Xia X, et al., 2023. Joint power control and passive beamforming optimization in RIS-assisted anti-jamming communication. *Front Inform Technol Electron Eng*, 24(12):1791-1802. https://doi.org/10.1631/FITEE.2200646

Liu YW, Xu JQ, Wang ZL, et al., 2023. Simultaneously transmitting and reflecting (STAR) RISs for 6G: fundamentals, recent advances, and future directions. *Front Inform Technol Electron Eng*, 24(12):1689-1707. https://doi.org/10.1631/FITEE.2300490

Lu HQ, Zeng Y, 2022a. Communicating with extremely large-scale array/surface: unified modeling and performance analysis. *IEEE Trans Wirel Commun*, 21(6):4039-4053. https://doi.org/10.1109/TWC.2021.3126384

Lu HQ, Zeng Y, 2022b. Delay alignment modulation: enabling equalization-free single-carrier communication. *IEEE Wirel Commun Lett*, 11(9):1785-1789. https://doi.org/10.1109/LWC.2022.3180736

Lu HQ, Zeng Y, 2023. Delay alignment modulation: manipulating channel delay spread for efficient single- and multi-carrier communication. *IEEE Trans Commun*, 71(11):6316-6331. https://doi.org/10.1109/TCOMM.2023.3306898

Lu HQ, Zeng Y, 2024. Delay-Doppler alignment modulation for spatially sparse massive MIMO communication. *IEEE Trans Wirel Commun*, 23(6):6000-6014. https://doi.org/10.1109/TWC.2023.3329487

Lu HQ, Zeng Y, Jin S, et al., 2024a. Single-carrier delay alignment modulation for multi-IRS aided communication. *IEEE Trans Wirel Commun*, 23(4):3267-3282. https://doi.org/10.1109/TWC.2023.3306899

Lu HQ, Zeng Y, You CS, et al., 2024b. A tutorial on near-field XL-MIMO communications towards 6G. *IEEE Commun Surv Tut*, 26(4):2213-2257. https://doi.org/10.1109/COMST.2024.3387749

Mukherjee A, Fakoorian SAA, Huang J, et al., 2014. Principles of physical layer security in multiuser wireless networks: a survey. *IEEE Commun Surv Tut*, 16(3):1550-

1573.
https://doi.org/10.1109/SURV.2014.012314.00178

Romero-Zurita N, Ghogho M, McLernon D, 2011. Physical layer security of MIMO frequency selective channels by beamforming and noise generation. IEEE 19th European Signal Processing Conf, p.829-833.

Sun GC, Shi H, Shang BL, et al., 2024. Secure transmission for active RIS-assisted THz ISAC systems with delay alignment modulation. *IEEE Commun Lett*, 28(5):1019-1023.
https://doi.org/10.1109/LCOMM.2024.3368532

Wang XW, Lu HQ, Zeng Y, 2023. Multi-user delay alignment modulation for millimeter wave massive MIMO. IEEE Global Communications Conf, p.6970-6975.
https://doi.org/10.1109/globecom54140.2023.10437061

Wang ZL, Mu XD, Liu YW, 2024. Bidirectional integrated sensing and communication: full-duplex or half-duplex? *IEEE Trans Wirel Commun*, 23(8):8184-8199.
https://doi.org/10.1109/TWC.2023.3344229

Wei L, Huang CW, Alexandropoulos GC, et al., 2023. Tri-polarized holographic MIMO surfaces for near-field communications: channel modeling and precoding design. *IEEE Trans Wirel Commun*, 22(12):8828-8842.
https://doi.org/10.1109/TWC.2023.3266298

Xiao ZQ, Zeng Y, 2023. Integrated sensing and communication with delay alignment modulation: performance analysis and beamforming optimization. *IEEE Trans Wirel Commun*, 22(12):8904-8918.
https://doi.org/10.1109/TWC.2023.3266758

Yang N, Wang LF, Geraci G, et al., 2015. Safeguarding 5G wireless communication networks using physical layer security. *IEEE Commun Mag*, 53(4):20-27.
https://doi.org/10.1109/MCOM.2015.7081071

Zeng Y, Yang L, Zhang R, 2018. Multi-user millimeter wave MIMO with full-dimensional lens antenna array. *IEEE Trans Wirel Commun*, 17(4):2800-2814.
https://doi.org/10.1109/TWC.2018.2803180

Zeng Y, Wu QQ, Zhang R, 2019. Accessing from the sky: a tutorial on UAV communications for 5G and beyond. *Proc IEEE*, 107(12):2327-2375.
https://doi.org/10.1109/JPROC.2019.2952892

Zhang GC, Wu QQ, Cui M, et al., 2019. Securing UAV communications via joint trajectory and power control. *IEEE Trans Wirel Commun*, 18(2):1376-1389.
https://doi.org/10.1109/TWC.2019.2892461

Zhang HY, Shlezinger N, Guidi F, et al., 2022. Beam focusing for near-field multiuser MIMO communications. *IEEE Trans Wirel Commun*, 21(9):7476-7490.
https://doi.org/10.1109/TWC.2022.3158894

Zhang JN, Zeng Y, 2024. Delay alignment modulation with hybrid beamforming for spatially sparse communications. IEEE Wireless Communications and Networking Conf, p.1-6.
https://doi.org/10.1109/WCNC57260.2024.10571150

Zhou G, Pan CH, Ren H, et al., 2021. Secure wireless communication in RIS-aided MISO system with hardware impairments. *IEEE Wirel Commun Lett*, 10(6):1309-1313.
https://doi.org/10.1109/LWC.2021.3064992

Zhou XY, McKay MR, 2010. Secure transmission with artificial noise over fading channels: achievable rate and optimal power allocation. *IEEE Trans Veh Technol*, 59(8):3831-3842.
https://doi.org/10.1109/TVT.2010.2059057

Zhu J, Schober R, Bhargava VK, 2014. Secure transmission in multicell massive MIMO systems. *IEEE Trans Wirel Commun*, 13(9):4766-4781.
https://doi.org/10.1109/TWC.2014.2337308

Zou YL, Zhu J, Wang XB, et al., 2016. A survey on wireless security: technical challenges, recent advances, and future trends. *Proc IEEE*, 104(9):1727-1765.
https://doi.org/10.1109/JPROC.2016.2558521